THE JOURNAL OF BIOLOGICAL CHEMISTRY VOL. 290, NO. 29, pp. 18227–18236, July 17, 2015

Astrocyte Elevated Gene-1 (AEG-1) Regulates Lipid Homeostasis*

Received for publication, April 27, 2015, and in revised form, June 4, 2015 Published, JBC Papers in Press, June 11, 2015, DOI 10.1074/jbc.M115.661801

Chadia L. Robertson[‡§1], Jyoti Srivastava[‡], Ayesha Siddiq[‡], Rachel Gredler[‡], Luni Emdad[‡], Devaraja Rajasekaran[‡], Maaged Akiel[‡], Xue-Ning Shen[‡], Frank Corwin[¶], Gobalakrishnan Sundaresan[¶], Jamal Zweit[¶], Colleen Croniger[‖], Xiaoli Gao[**], Shobha Ghosh[‡‡], Philip B. Hylemon[§§], Mark A. Subler[‡], Jolene J. Windle[‡¶¶], Paul B. Fisher[‡¶¶‖‖2], and Devanand Sarkar[‡¶¶‖‖3]

From the Departments of [‡]Human and Molecular Genetics, [§]Biochemistry, [¶]Radiology, [‡‡]Internal Medicine, and [§§]Microbiology and Immunology, the [¶¶]VCU Massey Cancer Center, and the [‖‖]VCU Institute of Molecular Medicine, Virginia Commonwealth University, Richmond, Virginia 23298, the [‖]Department of Nutrition, Case Western Reserve University, Cleveland, Ohio 44106, and the [**]Institutional Mass Spectrometry Laboratory, University of Texas Health Science Center, San Antonio, Texas 78229

Background: The physiological function of the oncogene astrocyte elevated gene-1 (AEG-1) was analyzed using a knock-out mouse (AEG-1KO).
Results: The AEG-1KO mouse shows a lean phenotype, which may be due to decreased intestinal fat absorption because of hyperactivation of LXR and PPARα.
Conclusion: A novel role of AEG-1 is identified, regulating lipid metabolism.
Significance: AEG-1 may play a role in regulating obesity and its associated disorders.

Astrocyte elevated gene-1 (AEG-1), also known as MTDH (metadherin) or LYRIC, is an established oncogene. However, the physiological function of AEG-1 is not known. To address this question, we generated an AEG-1 knock-out mouse (AEG-1KO) and characterized it. Although AEG-1KO mice were viable and fertile, they were significantly leaner with prominently less body fat and lived significantly longer compared with wild type (WT). When fed a high fat and cholesterol diet (HFD), WT mice rapidly gained weight, whereas AEG-1KO mice did not gain weight at all. This phenotype of AEG-1KO mice is due to decreased fat absorption from the intestines, not because of decreased fat synthesis or increased fat consumption. AEG-1 interacts with retinoid X receptor (RXR) and inhibits RXR function. In enterocytes of AEG-1KO mice, we observed increased activity of RXR heterodimer partners, liver X receptor and peroxisome proliferator-activated receptor-α, key inhibitors of intestinal fat absorption. Inhibition of fat absorption in AEG-1KO mice was further augmented when fed an HFD providing ligands to liver X receptor and peroxisome proliferator-activated receptor-α. Our studies reveal a novel role of AEG-1 in regulating nuclear receptors controlling lipid metabolism. AEG-1 may significantly modulate the effects of HFD and thereby function as a unique determinant of obesity.

The role of astrocyte elevated gene-1 (AEG-1)[4] (1, 2), also known as MTDH (metadherin) (3) and LYRIC (4), as an oncogene is well established (5–8). AEG-1 plays a crucial role in regulating tumor cell proliferation, invasion, and metastasis (3, 5, 8, 9) and positively contributes to tumor-associated angiogenesis, chemoresistance, and protection from apoptosis (6, 10–12). However, the physiological function of AEG-1 is still not known. The AEG-1 gene is present only in vertebrates, in which the protein is highly conserved, suggesting that AEG-1 evolved to perform specific functions in higher organisms (13). Analysis of AEG-1 expression during mouse development demonstrated AEG-1 expression in mid-to-hindbrain, frontonasal processes, limbs, and pharyngeal arches in the early development period from embryonic day 8.5 to 9.5 (14). At stages of embryonic day 12.5–18.5, AEG-1 expression was detected in the brain, the olfactory and skeletal systems, the skin, and the liver. Co-localization of AEG-1 expression was observed with the proliferation marker Ki-67, and it was hypothesized that AEG-1 might play a role in normal mouse development in the context of cell proliferation and differentiation (14).

Cholesterol and fatty acid absorption from the intestine is a complicated process involving specific transporters and efflux pumps, the expression of which is regulated by nuclear receptors, such as liver X receptor (LXR) and peroxisome proliferator-activated receptor (PPAR)-α (15, 16). In addition, metabolism of cholesterol and fatty acids in enterocytes determines their absorption into the lymph and blood and availability to other organs. Unesterified free cholesterol is taken up into the

* This work was supported, in whole or in part, by National Institutes of Health, NCI, Grants R01 CA138540 and R21 CA183954 (to D. S.) and National Institutes of Health Grant R01 CA134721 (to P. B. F.). This work was also supported in part by grants from The James S. McDonnell Foundation. The authors declare that they have no conflicts of interest with the contents of this article.
[1] Supported by National Institutes of Health, NIDDK, Grant T32DK007150.
[2] Holder of the Thelma Newmeyer Corman Chair in Cancer Research and a Samuel Waxman Cancer Research Foundation Investigator.
[3] The Harrison Foundation Distinguished Professor in Cancer Research and Blick scholar. To whom correspondence should be addressed: Dept. of Human and Molecular Genetics, Virginia Commonwealth University, 1220 East Broad St., P. O. Box 980035, Richmond, VA 23298. Tel.: 804-827-2339; Fax: 804-628-1176; E-mail: dsarkar@vcu.edu.

[4] The abbreviations used are: AEG-1, astrocyte elevated gene-1; RXR, retinoid X receptor; LXR, liver X receptor; PPAR, peroxisome proliferator-activated receptor; TG, triglyceride; HFD, high fat diet; AHH3, acetylated histone H3.

enterocytes by the cholesterol transporter NPC1L1, which can have three fates (15). Free cholesterol can be transported to the endoplasmic reticulum, where it is esterified by acyl-CoA: cholesterol acyltransferase 2 enzyme and then conjugated with ApoB48 to form chylomicron, which enters into the lymphatic system. Unesterified free cholesterol can be transported back to the intestinal lumen by apically located cholesterol pump ABCG5/ABCG8 heterodimer. Free cholesterol may be transported into the circulation as a constituent of HDL via ABCA1 located on the basolateral membrane of the enterocytes. When cellular oxysterols accumulate as a result of increasing concentrations of cholesterol, LXR activation, by cholesterol metabolites such as oxysterols (17), causes a net loss of cholesterol through down-regulation of NPC1L1 and reduction of acyl-CoA:cholesterol acyltransferase 2 enzyme activity as well as induction of ABCG5/ABCG8 and ABCA1 (18–20).

Important intestinal fatty acid transporters are: 1) fatty acid-binding protein, plasma membrane (FABPpm/Got2), located peripherally on the plasma membrane; 2) fatty acid translocase (FAT/CD36), an integral membrane glycoprotein; and 3) fatty acid transport protein subtype 4 (FATP4/Slc27a4), an integral membrane protein (21). In the intestinal lumen, triglyceride (TG) is broken down into free fatty acids by lipases. Once fatty acids enter into the enterocytes, cytoplasmic fatty acid-binding protein (FABPc) may transport them to the mitochondria for β-oxidation (22). The majority of fatty acids are re-esterified into TG and excreted into chylomicrons. In the enterocytes, PPARα promotes β-oxidation of fatty acids, thereby decreasing fatty acid absorption in the circulation (23, 24).

The present study unravels a novel physiological function of AEG-1 in lipid homeostasis by analyzing an AEG-1 knock-out (AEG-1KO) mouse. We previously documented that AEG-1 interacts with retinoid X receptor (RXR) (25), a master regulator of cell growth metabolism and development mediating the action of hormones, vitamins, and lipids (26, 27). RXR heterodimerizes with one-third of the 48 human nuclear receptor superfamily members, including LXR and PPARα (27). In the absence of their corresponding ligands, RXR heterodimers interact with co-repressors that maintain histones in a deacetylated state and inhibit transcription. Upon ligand binding, there is a conformational change so that the co-repressors are replaced by co-activators inducing histone acetylation and transcriptional activation. Co-activators, such as SRC-1, interact with nuclear receptors via an L*XX*LL motif (28). We documented that AEG-1 contains an L*XX*LL motif, through which it interacts with RXR that prevents co-activator recruitment and inhibits RXR function even in the presence of ligand (25). We now document augmented LXR and PPARα activity in enterocytes of AEG-1KO mice that hinders cholesterol and fatty acid absorption that may be one mechanism that leads to a lean phenotype. By regulating LXR and PPARα function, AEG-1 may significantly modulate the effects of a high fat diet and thus play a role in obesity-associated diseases.

Materials and Methods

Generation of AEG-1KO Mouse—The AEG-1KO mouse was generated in a C57BL/6:129/Sv background (25, 29). We have back-crossed the line to C57BL/6 for 10 generations and obtained similar results, which are described in this paper, for both the WT and AEG-1KO mice on the C57BL/6 background as on the C57BL/6:129/Sv background. The data presented in the figures were obtained from mice on the C57BL/6 background. All animal studies were approved by the institutional animal care and use committee at Virginia Commonwealth University and were conducted in accordance with the Animal Welfare Act, the Public Health Service Policy on Humane Care and Use of Laboratory Animals, and the United States Government Principles for the Utilization and Care of Vertebrate Animals Used in Testing, Research, and Training.

Measurement of Food Consumption and Body Weight—A measured amount of food was given to 4-week-old age-matched WT and AEG-1KO mice (n = 8/group) housed in individual cages. The amount of food consumed per week was determined by measuring the leftover food. Body weight was also measured weekly. The experiment was performed for 12 weeks. Food consumption was calculated by the amount of food (in g) consumed/g of body weight. The mice were fed regular chow. For the high fat diet (HFD) experiment, 8-week-old mice were fed a high fat and cholesterol-containing diet (Harlan; TD.88137) for 5 weeks. This diet contains 0.2% total cholesterol and 21% total fat by weight, which provides 42% kcal (4.5 kcal/g).

MRI of Total Body Fat Mapping—Male WT and AEG-1KO mice at 12 weeks of age were used (n = 6/group). Using a Bruker-Biospin Biospec console and a 7-tesla, 30-cm free bore magnet (Bruker Biospin), T2 weighted multislice spin echo images with and without fat suppression were acquired, covering the entire body from the base of skull to the tail, with a field of view of 4 × 4 cm and 256 × 256 matrix size. Animals were anesthetized with isoflurane during preparation (4%) and imaging (1%). The imaging parameters used were as follows: repetition time of 6.5 s, time of echo of 56 ms. The resultant two-dimensional images were exported and analyzed using ImageJ software (National Institutes of Health, Bethesda, MD). By subtracting the fat-suppressed images from the non-fat-suppressed images, fat-only images were produced, which were then used for region of interest analysis of the fat depots. Multiplying the area of the region of interest by slice thickness gave the volume.

Indirect Calorimetry—Male WT and AEG-1KO mice at 12 weeks of age were used (n = 6/group). VCO_2, VO_2, and respiratory quotient were measured using a four-chamber Columbus Instruments Comprehensive Lab Animal Monitoring System CLAMS/Oxymax (Columbus, OH) indirect calorimetry machine, which was calibrated based on the O_2 and CO_2 levels of the room dedicated for indirect calorimetry only. The mice were acclimated to the indirect calorimetry room for 1 week prior to the experiment. The oxygen consumption is calculated by taking the difference between the input oxygen flow and the output oxygen flow. Similarly, the carbon dioxide production is calculated by taking the difference between the output and input carbon dioxide flows. The calculations were analyzed as $VO_2 = V_i O2i - V_o O2o$, where V_i and V_o are the input and output ventilation rates (liters/min), and O2i and O2o are oxygen fractions at the input and output, and as $VCO_2 = V_o CO2o - V_i CO2i$, where V_i and V_o are the input and output

ventilation rates (liters/min), and CO2i and CO2o are carbon dioxide fractions at the input and output. The respiratory exchange ratio (RER) is simply the ratio between the carbon dioxide production and the oxygen consumption; thus, the equation is the following, RER = VCO_2/VO_2. Energy expenditure or heat is calculated before the application of any normalization or correction and, thus, reflects the exact heat of the subject. The calorific value (CV) is based on the observed respiratory exchange ratio. CV is then used with the observed oxygen consumption (VO_2) to calculate heat; the equations are as follows, heat = CV × VO_2 and CV = 3.815 + 1.232 × RER.

Measurement of Triglyceride Concentrations and Synthesis by Stable Isotopes—The Case Mouse Phenotyping Center measured the triglyceride content and newly synthesized triglyceride levels. In order to enrich the body water with ~2% ^{2}H, intraperitoneal injection of labeled water (20 μl × g^{-1} of body weight of 9 g/liter NaCl in 99% atomic percentage excess $2H_2O$) was administered to adult male mice, and they were returned to their cages and maintained on 5% ^{2}H-labeled drinking water for 5 days. The mice were sacrificed, and blood and tissue samples were collected and flash-frozen in liquid nitrogen. The samples were stored at −80 °C until analysis. Triglyceride concentrations and *de novo* lipogenesis were determined as described previously (30). Briefly, triglyceride from tissues was isolated, and labeled glycerol and palmitate were analyzed after derivatization by mass spectrometry. The ^{2}H-labeled triglyceride covalently linked to glycerol measures the amount of newly synthesized triglyceride, whereas the ^{2}H-labeled triglyceride covalently attached to palmitate indicates the amount of new palmitate. In mice given $2H_2O$ for 5 days, the contribution of *de novo* lipogenesis to the pool of triglyceride and palmitate was calculated using the following equation, % newly made palmitate = ((total ^{2}H-labeled palmitate × (^{2}H-labeled body water × *n*)) − 1) × 100, where *n* is the number of exchangeable hydrogens, which is assumed to be 22 (31, 32).

The percentage of total newly made triglyceride glycerol is calculated using the following equation, % total newly made triglyceride-glycerol = ((^{2}H-labeled triglyceride-glycerol × (^{2}H-labeled water × *n*)) − 1) × 100, where ^{2}H-labeled triglyceride-glycerol is the M1 isotopomer, ^{2}H-labeled water is the average amount labeled in a given mouse, and *n* is the exchange factor (experimentally determined from the M2/M1 ratio of triglyceride glycerol). We calculated the total triglyceride pool size (μmol/g of tissue) in the tissues using the following equation, total pool size of triglyceride = ((^{2}H-labeled triglyceride-glycerol × (^{2}H-labeled water × n)) − 1) × 100.

In Vivo Cholesterol Absorption—The fecal dual isotope ratio method (33) was used, in which WT and AEG-1KO mice were gavaged with 0.5 μCi of [^{14}C]cholesterol and 1 μCi of [^{3}H]sitostanol in 100 μl of soy bean oil. Mice were fed standard chow diet for 3 days, and the feces were collected daily. The radioactivity of the pooled fecal samples was determined by a scintillation counter. The percentage of cholesterol absorption was calculated as follows, ((^{14}C/^{3}H dosing mixture − ^{14}C/^{3}H feces)/(^{14}C/^{3}H dosing mixture) × 100.

In Vivo Fatty Acid Absorption—WT and AEG-1KO mice were fasted overnight and intravenously injected with 500 mg/kg tyloxapol to block serum lipase activity. After 30 min, mice were gavaged with fat emulsion containing 10 μCi of [^{3}H]triolein. Blood samples were collected from the tail vein at time 0 and hourly for 4 h. Serum radioactivity was determined by a scintillation counter (34).

Measurement of Fatty Acid β-Oxidation—Products of fatty acid β-oxidation was measured in fresh liver and small intestine homogenates using [^{14}C]palmitate as described (35).

Glucose Tolerance Test—Mice were fasted overnight (16 h), and glucose was injected intraperitoneally (1.5 g/kg). Blood samples were collected from the tail tip before and at 10, 30, 60, 90, and 120 min after the injection for the measurement of glucose with a glucometer.

Primary Hepatocyte Culture and Transfection Assays—Primary mouse hepatocytes were isolated as described (9) and were plated on collagen-coated dishes (BD BioCoat collagen type I, BD Biosciences) and cultured in Williams E medium (Sigma) containing $NaHCO_3$, L-glutamine, insulin (1.5 μM), and dexamethasone (0.1 μM). For transfections, 1 × 10^5 hepatocytes were plated in 24-well collagen-coated plates and transfected the next day using PromoFectin-Hepatocyte transfection reagent in a 9:1 ratio with firefly luciferase reporter plasmid containing responsive elements (pGL3.luc, pGL3.*LXRE*.luc, and pGL3.*PPRE*.luc) and *Renilla* luciferase reporter plasmid (pGL3.renilla.luc). After 48 h, cells were incubated in the presence or absence of the respective ligands (T0901317 (5 μM) and CP775146 (2.5 μM)) for another 24 h. Luciferase assays were measured using the Dual-Luciferase Reporter Assay kit (Promega) following the manufacturer's protocol, and firefly luciferase activity was normalized by *Renilla* luciferase activity. Each experiment was performed in triplicates and three times to calculate means and S.D. values.

Total RNA Extraction, cDNA Preparation, and Real-time PCR—Total RNA was extracted from hepatocytes or mouse tissues using the Qiagen miRNAeasy minikit (Qiagen, Hilden, Germany). cDNA preparation was done using the ABI cDNA synthesis kit (Applied Biosystems, Foster City, CA). RT-PCR was performed using an ABI ViiA7 fast real-time PCR system and Taqman gene expression assays according to the manufacturer's protocol (Applied Biosystems). The expression level of each gene was determined by the $\Delta\Delta CT$ method and was normalized by the level of GAPDH. The level of untreated control for each gene was considered as 1 to determine the -fold difference.

Chromatin Immunoprecipitation (ChIP) Assay—12-week-old WT and AEG-1KO littermates ($n = 3$) were treated with the LXR agonist T0901317 (30 μg/g) by a single oral gavage. 24 h later, the animals were euthanized, and livers were immediately removed. A ChIP assay was performed using a SimpleChIP Plus kit (Cell Signaling Technology, Danvers, MA) according to the manufacturer's instructions (25). The antibodies used were rabbit anti-LXRα (Santa Cruz Biotechnology, Inc.), anti-acetylated histone H3 (AHH3), and anti-SRC-1 (Cell Signaling). Normal rabbit IgG was used as control. DNA was purified, and quantitative PCR was performed using Power SYBR Green PCR Mastermix (Applied Biosystems) on the ABI ViiA7 fast real-time PCR system according to the manufacturer's protocol (Applied Biosystems). PCR efficiencies of primers were examined by a standard curve of serial-diluted liver extract input and

melting curve functionality. The primers used were Abca1 forward (5′-GAACGAGCTTTTCCCCTTTC-3′) and Abca1 reverse (5′-CCCGGCCTCTGTTTATGTAG-3′).

Western Blot Analysis—Western blot analysis were performed as described previously (5). The following primary antibodies were used: anti-ABCA1 (mouse; Santa Cruz Biotechnology; catalogue no. sc-58219; 1:2000), anti-CPT1A (rabbit; Proteintech; catalogue no. 15184-1-AP; 1:1000), anti-NPC1L1 (rabbit; Cell Signaling Technology; catalogue no. 5058; 1:500), anti-PPARα (rabbit; Santa Cruz Biotechnology; catalogue no. sc-9000; 1:500), anti-LXR (rabbit; Santa Cruz Biotechnology; catalogue no. sc-13068; 1:1000), anti-AEG-1 (chicken; in-house; 1:3000) and anti-GAPDH (mouse; Santa Cruz Biotechnology; catalogue no. sc-166545; 1:2500).

Statistical Analysis—Data were represented as the mean ± S.E. and analyzed for statistical significance using one-way analysis of variance followed by Newman-Keuls test as a post hoc test. A p value of <0.05 was considered as significant.

Results

AEG-1KO Mice Are Lean and Survive Longer—We generated an AEG-1KO mouse in which the promoter region, exon 1, and part of intron 1 of the AEG-1 gene was deleted using a Cre-loxP system (25, 29). AEG-1KO mice were viable and fertile, although the litter size was smaller than expected. Both WT and KO mice developed normally to full adulthood, indicating that AEG-1 is probably not involved in developmental regulation. Histological analysis of the internal organs of the adult mice also did not reveal any significant and noticeable difference between WT and AEG-1KO mice (29).

However, a marked difference in body weight gain was observed between age-matched WT and AEG-1KO mice. We performed weekly monitoring of body weight starting at 4 weeks of age when the mice were weaned. Over the next 12 weeks, the average body weight gain by each WT mouse was ~14 g, whereas that in AEG-1KO mice was only ~4 g (Fig. 1*A*). During this period, the food consumption (g of food/g of body weight) was similar in both groups (Fig. 1*B*). The substantial difference in body weight gain continued with age (Fig. 1, *C* and *D*) and was more pronounced in male mice compared with female mice (Fig. 1, *C* and *D*). MRI analysis of the mice demonstrated a significant decrease in visceral, subcutaneous, and intramuscular fat in the AEG-1KO mice compared with WT mice (Fig. 2, *A* and *B*). Histologically, adipocytes in white and brown adipose tissues were larger and more abundant in WT mice *versus* AEG-1KO mice (Fig. 2*C*). Aged (15 months old) WT mice demonstrated steatotic changes in the liver, whereas no such change was observed in AEG-1KO mice (Fig. 2*D*). The mice were monitored until 24 months, by which time point 19 of 21 WT mice had died, whereas a significant survival benefit was observed in the leaner AEG-1KO mice, of which only 3 of 20 mice had died (Fig. 2*E*). No significant difference was observed in glucose tolerance, indicating that insulin signaling is functional in AEG-1KO mice (Fig. 2*F*). Glucose uptake in peripheral tissues by an [^{18}F]FDG uptake assay also did not show a difference between WT and AEG-1KO mice (data not shown).

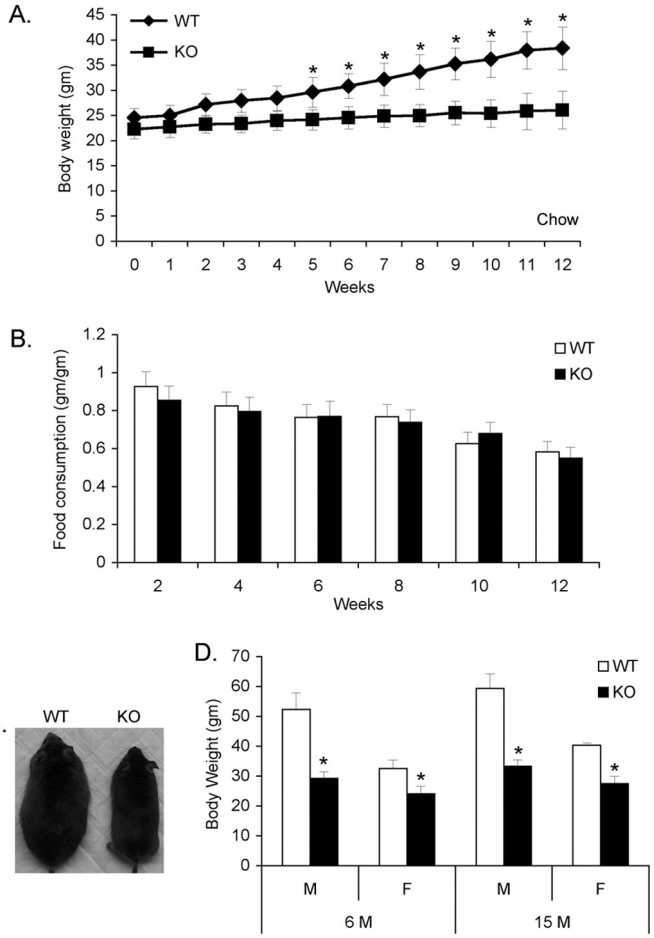

FIGURE 1. **AEG-1KO mice are smaller than WT mice.** *A*, weekly body weight gain (n = 8/group). *B*, biweekly food consumption (n = 8/group). *C*, photograph of mice at 15 months of age. *D*, body weight of male (*M*) and female (*F*) mice at 6 and 15 months of age (n = 12/group). For graphs, the data represent mean ± S.E. (*error bars*). *, $p < 0.05$.

Intestinal Fat Absorption Is Inhibited in AEG-1KO Mice—The profound lack of fat in AEG-1KO mice may be due to 1) defects in fat synthesis, 2) increased energy expenditure (fat burning), and/or 3) decreased fat absorption from the intestine. To address this issue, we first measured serum total TG and cholesterol levels, both of which were significantly lower in AEG-1KO compared with WT mice (Fig. 3*A*). Levels of newly synthesized TG and palmitate in liver and muscle of WT and AEG-1KO mice showed no significant differences (Fig. 3, *B* and *C*). An indirect calorimetry analysis measuring O_2 consumption and CO_2 production did not reveal any increased expenditure in AEG-1KO mice (Fig. 3*D*). Rather, AEG-1KO mice demonstrated a small but statistically significant decrease in energy expenditure compared with WT mice (Fig. 3, *D* and *E*). No difference was observed in UCP1 (uncoupling protein 1) levels in white and brown adipose tissue of WT and AEG-1KO mice (data not shown). Both cholesterol and fatty acid absorption by the intestine were markedly inhibited in AEG-1KO *versus* WT mice (Fig. 3, *F* and *G*). Cholesterol absorption was measured by gavaging [^{14}C]cholesterol and then measuring radioactivity in the feces, whereas fatty acid absorption was quantified by gavaging [^{3}H]triolein and then temporally measuring plasma radioactivity. Collectively, the lack of body fat and lean pheno-

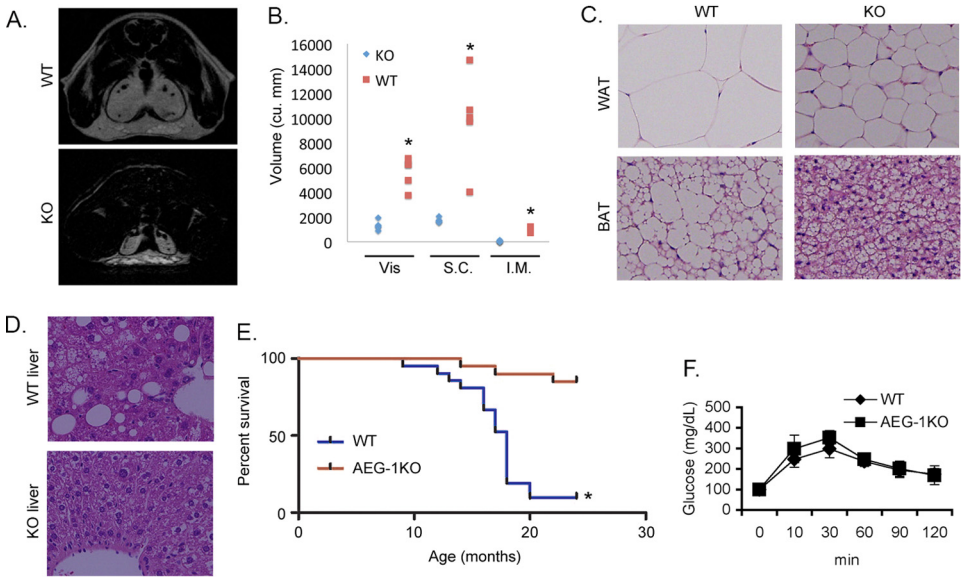

FIGURE 2. **AEG-1KO mice have less body fat compared with WT mice.** *A*, representative MRI image of 5-month-old mice. *B*, quantification of body fat distribution determined by MRI ($n = 5$/group). *C*, H&E staining of white adipose tissue (*WAT*) and brown adipose tissue (*BAT*) at 15 months. *D*, H&E staining of liver at 15 months. *E*, Kaplan-Meier survival curve at 24 months ($n = 21$ for WT and $n = 20$ for AEG-1KO). In the graphs, the data represent mean ± S.E. (*error bars*). *, $p < 0.05$. *F*, blood glucose was measured at the indicated time points after intraperitoneal injection of a bolus of glucose in overnight fasted mice. The data represent mean ± S.E. ($n = 5$/group).

type in AEG-1KO mice may be explained by reduced cholesterol and TG absorption from the intestine.

We next evaluated the effect of feeding an HFD on the lean phenotype of AEG-1KO mice, starting at 8 weeks of age. Over a period of 5 weeks, each WT mouse gained ~11 g of body weight on average, whereas no weight gain was observed in AEG-1KO mice (Fig. 3*H*). Post-mortem evaluation revealed evidence of steatosis in the liver of WT mice but not in AEG-1KO mice (Fig. 3*I*). These findings support the hypothesis that inhibition of intestinal fat absorption results in lean phenotype in AEG-1KO mice so that even feeding HFD could not induce a gain of body weight.

LXR and PPARα Activities Are Augmented in the Intestine of AEG-1KO Mice—We next searched for the molecular mechanism conferring the phenotypes of AEG-1KO mice. We have identified a novel interaction between AEG-1 and RXR that interferes with co-activator recruitment and inhibits RXR-mediated transcriptional regulation by its heterodimer partners (25). The phenotypes of the AEG-1KO mice may be explained by activation of LXR and PPARα, heterodimer partners of RXR, in the intestines. In enterocytes, activation of LXR inhibits cholesterol absorption by down-regulating cholesterol transporter Npc1l1 and up-regulating cholesterol efflux proteins, Abca1, Abcg5, and Abcg8 (15). Activation of PPARα in the enterocytes promotes β-oxidation of absorbed fatty acids, thereby down-regulating fatty acid absorption into the circulation (23, 24). Products of cholesterol metabolism, such as oxysterols, function as ligands for LXR, whereas fatty acids and fatty acid derivatives are endogenous ligands for PPARα (17, 36). HFD provides ligands to both LXR and PPARα, thereby accentuating this effect with resultant almost complete inhibition of fat absorption.

To confirm our hypothesis, we first checked LXR and PPARα activity by luciferase reporter assays in WT and AEG-1KO hepatocytes upon treatment with synthetic ligands T0901317 (5 μM) and CP775146 (2.5 μM), respectively. Both basal and ligand-dependent LXR and PPARα activities were significantly higher in AEG-1KO hepatocytes compared with WT hepatocytes (Fig. 4, *A* and *B*). Analysis of LXR expression showed an increased LXR level in the intestines of AEG-1KO mice compared with WT (Fig. 4*C*) We treated WT and AEG-1KO mice with T0901317 for 24 h and analyzed recruitment of LXR, AHH3, and co-activator SRC-1 on the promoter region of LXR target gene Abca1 by a ChIP assay using liver samples. A significant increase in recruitment of LXR, AHH3, and SRC-1 was observed in AEG-1KO livers *versus* WT livers, confirming that our previous *in vitro* observation (25) holds true in an *in vivo* situation (Fig. 4*D*). We checked the expression of LXR target genes in the small intestine of WT and AEG-1KO mice fed regular chow or HFD. The basal expression level of Abca1 was markedly higher in AEG-1KO mice compared with WT mice (Fig. 4*E*). With regular chow, the heterodimeric efflux pump Abcg5 and Abcg8 showed small but significant increase in AEG-1KO *versus* WT mice. Upon HFD treatment, the expression of all three genes was significantly induced in both WT and AEG-1KO mice. However, the magnitude of induction was significantly robust, especially for Abca1, in AEG-1KO mice compared with WT mice (Fig. 4*F*). Conversely, the basal expression level of the cholesterol transporter Npc1l1 was significantly lower in AEG-1KO mice *versus* WT mice, and upon HFD treatment, this decrease was further accentuated (Fig. 4*E*). The increased levels of the cholesterol efflux pumps and decrease in the cholesterol transporter explain the inhibition of intestinal cholesterol absorption in AEG-1KO mice, which is further accentuated upon HFD treatment that provides ligands to LXR, augmenting its effects.

We next analyzed the expression levels of PPARα target genes that regulate β-oxidation of fatty acids in the small intes-

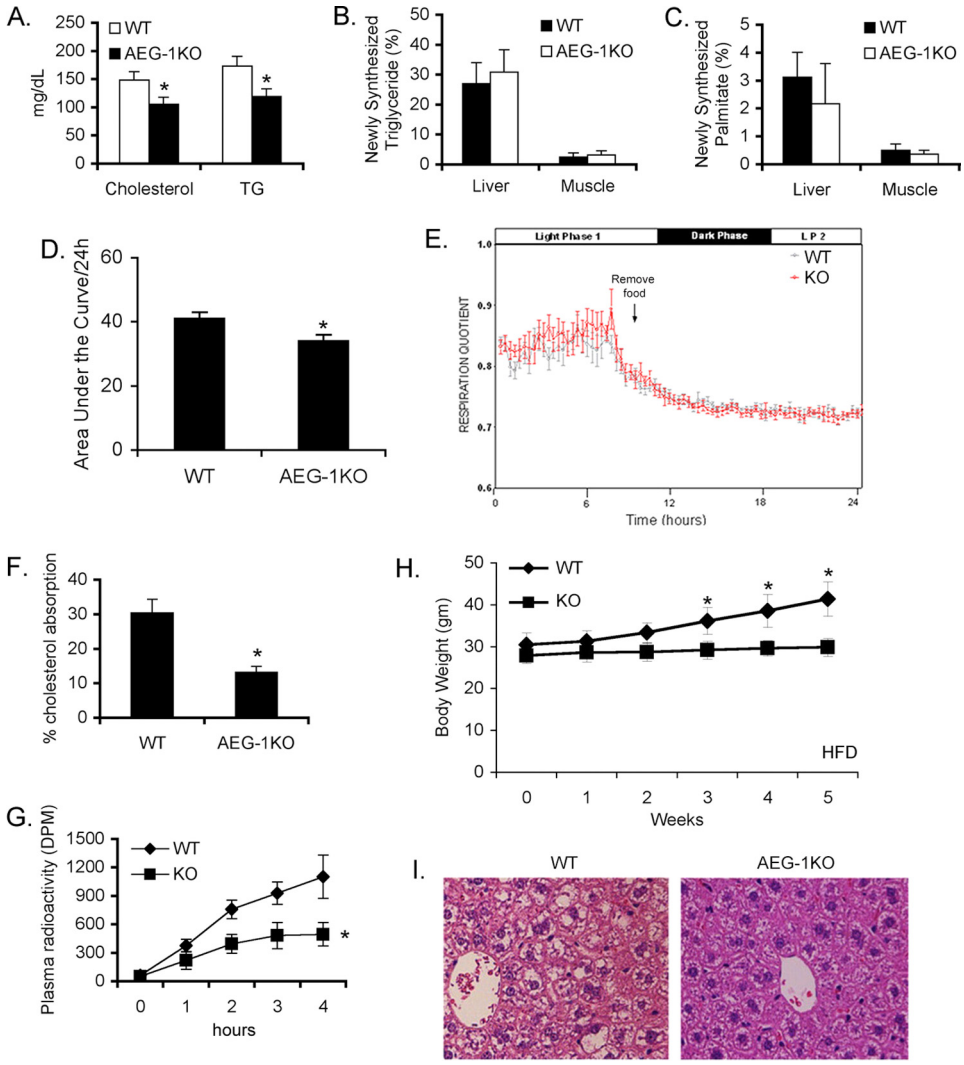

FIGURE 3. **Intestinal fat absorption is inhibited in AEG-1KO mouse.** *A*, serum total cholesterol and TG levels ($n = 5$/group). *B* and *C*, measurement of newly synthesized triglyceride (*B*) and palmitate (*C*). *D* and *E*, indirect calorimetry analysis measuring O_2 consumption and CO_2 production ($n = 6$/group). Area under the curve (*D*) and respiration quotient (*E*) plots are shown. *F*, measurement of cholesterol absorption from the intestine after gavaging [^{14}C]cholesterol and then measuring radioactivity in the feces. *G*, measurement of fatty acid absorption by gavaging [^{3}H]triolein and then temporally measuring plasma radioactivity. *H*, weekly body weight gain upon feeding HFD ($n = 8$). *I*, H&E staining of liver sections of mice fed HFD. In the graphs, the data represent mean ± S.E. (*error bars*). *, $p < 0.05$.

tine and liver. For the mitochondrial β-oxidation pathway, we analyzed Cpt1a, the rate-limiting enzyme in the carnitine-dependent transport of fatty acids across the mitochondrial membrane, and Acadl and Acadm, which catalyze the initial steps of fatty acid β-oxidation (37). For peroxisomal β-oxidation, we analyzed Acox1, the first enzyme in this pathway (37). In standard chow-fed mice, Cpt1a and Acadl expression levels were significantly higher in the small intestine, and Cpt1a, Acadl, and Acadm levels were significantly higher in the liver of AEG-1KO mice *versus* WT mice (Fig. 5, *A* and *B*). There were no significant differences in the Acox1 levels between AEG-1KO and WT mice in either organ. With HFD treatment, a significant induction of all four genes was observed in both the small intestine and liver of WT mice. In the small intestine of AEG-1KO mice, HFD treatment resulted in a significant induction of all four genes, which was significantly more pronounced than the induction seen in WT mice (Fig. 5*A*). However, HFD treatment did not result in further induction of these genes in the liver of AEG-1KO mice (Fig. 5*B*). The basal Ppara level was significantly higher in the small intestine and liver of AEG-1KO mice *versus* WT mice (Fig. 5, *C* and *D*). HFD treatment resulted in induction of Ppara in both WT and AEG-1KO liver and small intestine. However, the magnitude of this induction was much more pronounced in the small intestine of AEG-1KO mice *versus* WT mice (Fig. 5*C*). Additionally, in AEG-1KO mice, the HFD-mediated induction of Ppara was more robust in the small intestine than in the liver (Fig. 5, *C* and *D*). No significant difference was observed in the level of Pparg and Ppargc1, the co-activator for PPAR (Fig. 5, *C* and *D*). The changes in LXR and PPARα target genes in the small intestines of chow- and HFD-fed mice were confirmed at the protein level by Western blot analysis (Fig. 5*E*). We measured products of fatty acid β-oxidation in fresh liver and small intestine homogenates using [^{14}C]palmitate (35). Acetyl-CoA, generated by β-oxidation, enters the tricarboxylic acid cycle to generate CO_2. [^{14}C]Palmitate that does not

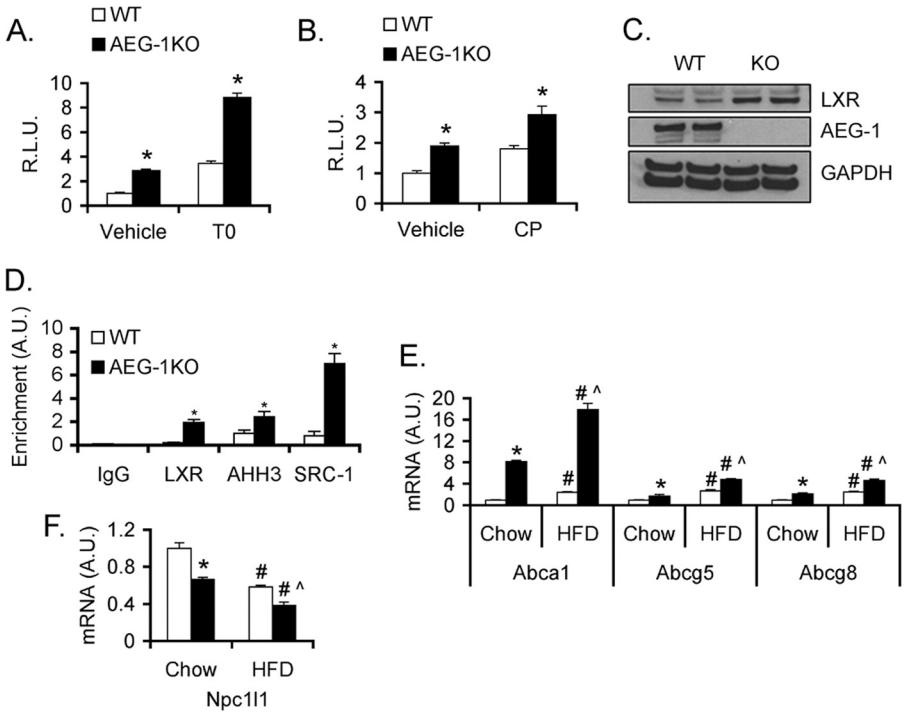

FIGURE 4. **LXR is activated in the intestine of AEG-1KO mice.** *A* and *B*, LXRE (*A*) and PPARE (*B*) luciferase activity was determined in WT and AEG-1KO hepatocytes upon treatment with LXR ligand, T0901317 (5 μM), and PPARα ligand, CP775146 (2.5 μM), respectively. *R.L.U.*, relative luciferase units. *C*, the expression of the indicated proteins was detected by Western blot in the intestines of WT and AEG-1KO mice. Two independent mice of each group are shown. *D*, ChIP assays were performed using anti-LXRα, anti-AHH3, and anti-SRC-1 antibodies using T0901317-treated WT and AEG-1KO livers and PCR primers amplifying promoter regions of the *Abca1* gene. Normal rabbit IgG was used as control, and the data were normalized by results obtained using normal IgG. *E* and *F*, expression of the indicated genes by Taqman quantitative RT-PCR in chow- and HFD-fed small intestine. The data represent mean $\pm$ S.E. (*error bars*). *, $p < 0.05$ *versus* the corresponding data point in WT mice; #, $p < 0.05$ chow *versus* HFD in WT mice; [caret], $p < 0.05$ chow *versus* HFD in AEG-1KO mice. *A.U.*, arbitrary units.

get oxidized forms acid-soluble metabolites. Fatty acid β-oxidation was significantly increased in the liver and small intestine of AEG-1KO mouse *versus* WT (Fig. 5*F*). Collectively, these findings suggest that under basal conditions, higher levels of PPARα and its target genes in the small intestine of AEG-1KO mice confer increased fatty acid β-oxidation in the enterocytes, resulting in decreased fatty acid absorption. This effect is further accentuated upon HFD treatment that provides ligands to PPARα, thus augmenting levels of both Ppara and its target genes. The lack of absorption of fatty acids from the intestines upon HFD treatment results in decreased delivery of PPARα ligands to the liver, so that there was no further induction by HFD compared with the chow diet. No significant difference was observed in the expression levels of enterocyte fatty acid transporters, FABPpm/Got2, FAT/Cd36, and FATP4/Slc27a4 in WT and AEG-1KO mice (Fig. 5*G*) with regular chow or HFD, further indicating that fatty acid transport from the lumen to the enterocyte is normal, and it is enhanced β-oxidation that abrogates absorption to the plasma. We also did not observe a significant difference in bile acid composition between WT and AEG-1KO mice (Fig. 5*H*), indicating that anomalies in bile composition may not be a potential mechanism of decreased fat absorption.

Discussion

This work provides a conceptual framework for understanding the role of AEG-1 in normal physiology. Up until now, AEG-1 has been known only for its role in tumorigenesis. Here for the first time, we show that the lack of AEG-1 in mice augments LXR and PPARα activity, thereby preventing fat absorption from the intestine. We observed an increase in LXR and PPARα levels in the intestines of AEG-1KO *versus* WT mice. It has been documented that LXR and PPARα may indirectly regulate each other (38). As such, relief of AEG-1-induced suppression of their activity may lead to increased expression of these transcription factors. One limitation of our study is that we performed ChIP analysis using liver tissue from mice that were treated with the LXR ligand T0901317. Ideally, this study should have been performed using intestinal tissue. However, we encountered several technical hurdles. The presence of only a single layer of enterocytic cells in the intestine and that of tough muscular and peritoneal tissue resulted in extraction of a very limited amount of DNA that precluded effective use for ChIP analysis. To overcome this limitation, we performed the assay using liver tissue as a "proof of principle" using the same LXR target gene that is relevant for the intestine. We documented increased recruitment of SRC-1 to the promoter of the Abca1 gene in the AEG-1KO mouse that provided support to our hypothesis. Thus, it may be argued that AEG-1 regulates LXR and PPARα both at a functional level and at the level of expression. We also did not observe difference in bile acid composition between WT and AEG-1KO mouse. Bile acid metabolism is primarily regulated by FXR, another RXR heterodimer partner. As yet, why AEG-1 knockdown did not affect bile acid

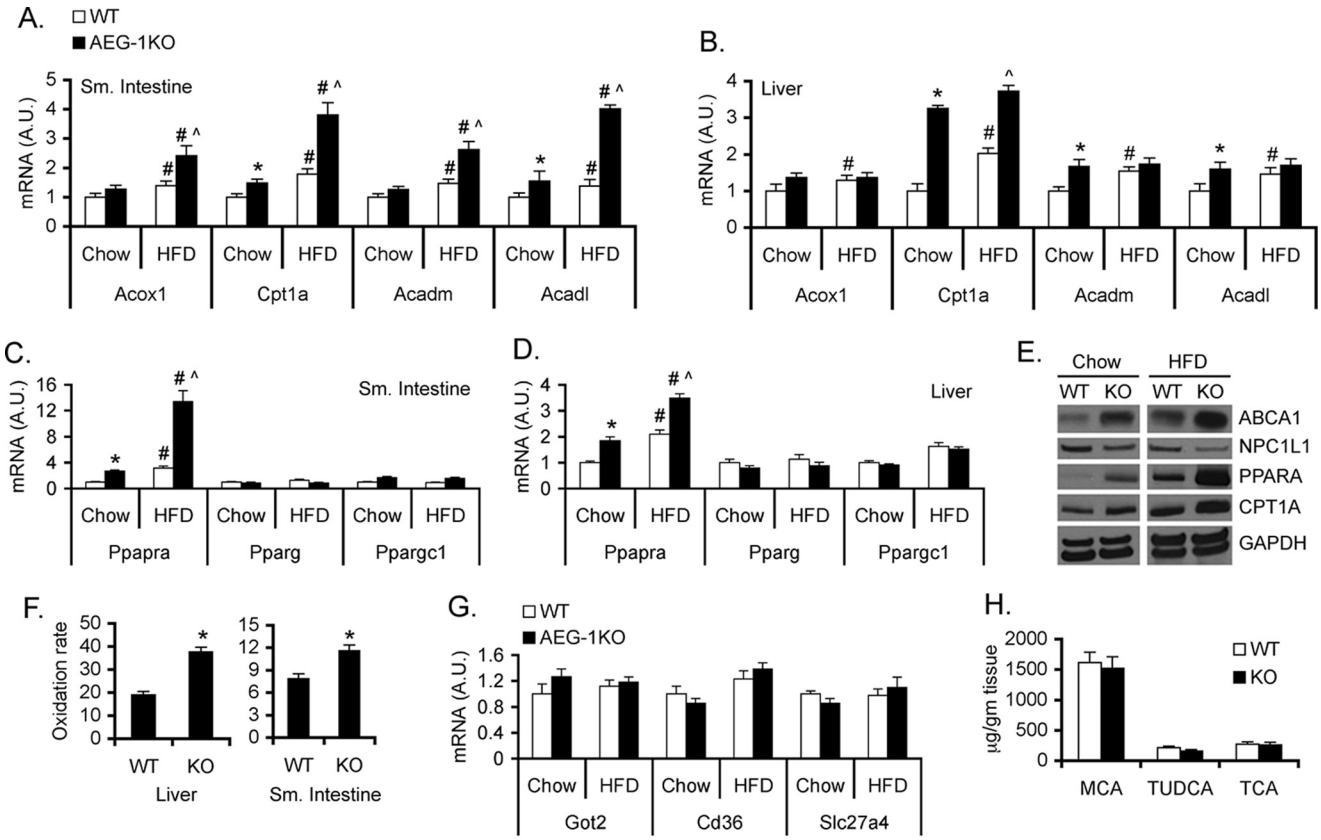

FIGURE 5. **PPARα is activated in the intestine of AEG-1KO mice.** *A–D*, expression of the indicated genes by Taqman quantitative RT-PCR in chow- and HFD-fed small intestine (*A* and *C*) and chow- and HFD-fed liver (*B* and *D*). The data represent mean ± S.E. (*error bars*). *, $p < 0.05$ *versus* corresponding data point in WT mice; #, $p < 0.05$ chow *versus* HFD in WT mice; [caret], $p < 0.05$ chow *versus* HFD in AEG-1KO mice. *White bars*, WT; *black bars*, AEG-1KO. *E*, expression of the indicated proteins was checked in the small intestines of chow- or HFD-fed WT and AEG-1KO mice by Western blot analysis. *F*, fatty acid β-oxidation is increased in AEG-1KO mice. Fresh liver and small intestine homogenates were used with [^{14}C]palmitate as substrate. Oxidation rate is nmol/mg/min. The data represent mean ± S.E. *, $p < 0.01$. *G*, expression of the indicated genes was measured in the small intestines of the chow- and HFD-fed WT and AEG-1KO mice. *H*, bile acid levels in the gallbladder of adult mice. *MCA*, muricholic acid; *TUDCA*, tauroursodeoxycholic acid; *TCA*, taurocholic acid. For *G* and *H*, the data represent mean ± S.E. For *A–D* and *F–H*, $n = 4$/group. *A.U.*, arbitrary units.

composition is not clear. Studies are being performed to obtain more in depth insights into the molecular mechanism of AEG-1-mediated nuclear factor regulation.

It should be noted that abrogation of intestinal fat absorption may be one of several mechanisms that contribute to the lean phenotype in the AEG-1KO mouse. AEG-1 is expressed in the neurons, and knocking out AEG-1 in the brain may also cause a central effect eliciting the observed phenotypes. We did not observe differences in food consumption between WT and AEG-1KO mouse, suggesting that AEG-1 may not regulate feeding behavior. However, the possibility of dysregulation of a plethora of RXR heterodimer partners in the brain contributing to the lean phenotype should not be ignored. Further studies need to be carried out to elucidate a potential role of AEG-1 in regulation of brain function.

In addition to the lean phenotype, we observed that although AEG-1KO mice were viable and fertile, the litter sizes were very small (1–2 pups/litter). Further, even litters generated by crossing AEG-$1^{+/-}$ breeding pairs were very small (2–3 pups/litter), which precluded generating large numbers of WT and AEG-1KO mice as littermates. A recent study has demonstrated a role of AEG-1 in male infertility, thereby explaining the phenotype (39). To obtain a sufficient number of AEG-1KO mice for statistical analysis, some of the experiments were carried out with age-matched mice generated by breeding WT and AEG-1KO mice separately. However, it should be noted that the same phenotypes were observed in AEG-1KO mice generated from AEG-$1^{+/-}$ × AEG-$1^{+/-}$ matings as from AEG-1KO × AEG-1KO matings. Thus, our findings are not restricted to strains or littermates. AEG-1KO mice live significantly longer than WT. Caloric restriction is the most effective way of increasing longevity (40). The inherent inability of AEG-1KO mice to accumulate fat may provide them with the beneficial effect of longer life. We previously documented that AEG-1 is fundamentally required for NF-κB activation and, compared with WT mice AEG-1KO mice, showed profound inhibition in aging-associated inflammation (29). This factor may also contribute to increased survival in AEG-1KO mice.

Taken together, these findings provide evidence that AEG-1 plays an essential role in maintaining homeostasis in lipid metabolism. These findings have important implications for a number of different pathological conditions, including obesity and non-alcoholic fatty liver disease, where AEG-1 overexpression may facilitate increased fat availability and may contribute to fat accumulation and ultimately cirrhosis of the liver and obesity-associated cancers. Our findings highlight AEG-1 as a new potential target to therapeutic intervention of obesity-associated illnesses.

Author Contributions—C. L. R. designed and performed experiments, analyzed the data, and wrote the manuscript. J. S., A. S., R. G., L. E., D. R., M. A., X. S., F. C., G. S., J. Z., C. C., X. G., M. A. S., and J. J. W. designed and performed experiments and analyzed data. S. G., P. B. H., and P. B. F. interpreted data and edited the manuscript. D. S. designed and performed experiments, analyzed data, and edited the manuscript.

References

1. Su, Z. Z., Kang, D. C., Chen, Y., Pekarskaya, O., Chao, W., Volsky, D. J., and Fisher, P. B. (2002) Identification and cloning of human astrocyte genes displaying elevated expression after infection with HIV-1 or exposure to HIV-1 envelope glycoprotein by rapid subtraction hybridization, RaSH. *Oncogene* **21,** 3592–3602
2. Kang, D. C., Su, Z. Z., Sarkar, D., Emdad, L., Volsky, D. J., and Fisher, P. B. (2005) Cloning and characterization of HIV-1-inducible astrocyte elevated gene-1, AEG-1. *Gene* **353,** 8–15
3. Brown, D. M., and Ruoslahti, E. (2004) Metadherin, a cell surface protein in breast tumors that mediates lung metastasis. *Cancer Cell* **5,** 365–374
4. Britt, D. E., Yang, D. F., Yang, D. Q., Flanagan, D., Callanan, H., Lim, Y. P., Lin, S. H., and Hixson, D. C. (2004) Identification of a novel protein, LYRIC, localized to tight junctions of polarized epithelial cells. *Exp. Cell Res.* **300,** 134–148
5. Yoo, B. K., Emdad, L., Su, Z. Z., Villanueva, A., Chiang, D. Y., Mukhopadhyay, N. D., Mills, A. S., Waxman, S., Fisher, R. A., Llovet, J. M., Fisher, P. B., and Sarkar, D. (2009) Astrocyte elevated gene-1 regulates hepatocellular carcinoma development and progression. *J. Clin. Invest.* **119,** 465–477
6. Emdad, L., Lee, S. G., Su, Z. Z., Jeon, H. Y., Boukerche, H., Sarkar, D., and Fisher, P. B. (2009) Astrocyte elevated gene-1 (AEG-1) functions as an oncogene and regulates angiogenesis. *Proc. Natl. Acad. Sci. U.S.A.* **106,** 21300–21305
7. Sarkar, D., and Fisher, P. B. (2013) AEG-1/MTDH/LYRIC: clinical significance. *Adv. Cancer Res.* **120,** 39–74
8. Hu, G., Chong, R. A., Yang, Q., Wei, Y., Blanco, M. A., Li, F., Reiss, M., Au, J. L., Haffty, B. G., and Kang, Y. (2009) MTDH activation by 8q22 genomic gain promotes chemoresistance and metastasis of poor-prognosis breast cancer. *Cancer Cell* **15,** 9–20
9. Srivastava, J., Siddiq, A., Emdad, L., Santhekadur, P. K., Chen, D., Gredler, R., Shen, X.-N., Robertson, C. L., Dumur, C. I., Hylemon, P. B., Mukhopadhyay, N. D., Bhere, D., Shah, K., Ahmad, R., Giashuddin, S., Stafflinger, J., Subler, M. A., Windle, J. J., Fisher, P. B., and Sarkar, D. (2012) Astrocyte elevated gene-1 (AEG-1) promotes hepatocarcinogenesis: novel insights from a mouse model. *Hepatology* **56,** 1782–1791
10. Yoo, B. K., Gredler, R., Vozhilla, N., Su, Z. Z., Chen, D., Forcier, T., Shah, K., Saxena, U., Hansen, U., Fisher, P. B., and Sarkar, D. (2009) Identification of genes conferring resistance to 5-fluorouracil. *Proc. Natl. Acad. Sci. U.S.A.* **106,** 12938–12943
11. Yoo, B. K., Chen, D., Su, Z.-Z., Gredler, R., Yoo, J., Shah, K., Fisher, P. B., and Sarkar, D. (2010) Molecular mechanism of chemoresistance by astrocyte elevated gene-1 (AEG-1). *Cancer Res.* **70,** 3249–3258
12. Lee, S. G., Su, Z. Z., Emdad, L., Sarkar, D., Franke, T. F., and Fisher, P. B. (2008) Astrocyte elevated gene-1 activates cell survival pathways through PI3K-Akt signaling. *Oncogene* **27,** 1114–1121
13. Lee, S. G., Kang, D. C., DeSalle, R., Sarkar, D., and Fisher, P. B. (2013) AEG-1/MTDH/LYRIC, the beginning: initial cloning, structure, expression profile, and regulation of expression. *Adv. Cancer Res.* **120,** 1–38
14. Jeon, H. Y., Choi, M., Howlett, E. L., Vozhilla, N., Yoo, B. K., Lloyd, J. A., Sarkar, D., Lee, S. G., and Fisher, P. B. (2010) Expression patterns of astrocyte elevated gene-1 (AEG-1) during development of the mouse embryo. *Gene Expr. Patterns* **10,** 361–367
15. Bonamassa, B., and Moschetta, A. (2013) Atherosclerosis: lessons from LXR and the intestine. *Trends Endocrinol. Metab.* **24,** 120–128
16. Wahli, W., and Michalik, L. (2012) PPARs at the crossroads of lipid signaling and inflammation. *Trends Endocrinol. Metab.* **23,** 351–363
17. Janowski, B. A., Willy, P. J., Devi, T. R., Falck, J. R., and Mangelsdorf, D. J. (1996) An oxysterol signalling pathway mediated by the nuclear receptor LXR α. *Nature* **383,** 728–731
18. Venkateswaran, A., Laffitte, B. A., Joseph, S. B., Mak, P. A., Wilpitz, D. C., Edwards, P. A., and Tontonoz, P. (2000) Control of cellular cholesterol efflux by the nuclear oxysterol receptor LXR α. *Proc. Natl. Acad. Sci. U.S.A.* **97,** 12097–12102
19. Repa, J. J., Turley, S. D., Lobaccaro, J. A., Medina, J., Li, L., Lustig, K., Shan, B., Heyman, R. A., Dietschy, J. M., and Mangelsdorf, D. J. (2000) Regulation of absorption and ABC1-mediated efflux of cholesterol by RXR heterodimers. *Science* **289,** 1524–1529
20. Repa, J. J., Berge, K. E., Pomajzl, C., Richardson, J. A., Hobbs, H., and Mangelsdorf, D. J. (2002) Regulation of ATP-binding cassette sterol transporters ABCG5 and ABCG8 by the liver X receptors α and β. *J. Biol. Chem.* **277,** 18793–18800
21. Masson, C. J., Plat, J., Mensink, R. P., Namiot, A., Kisielewski, W., Namiot, Z., Füllekrug, J., Ehehalt, R., Glatz, J. F., and Pelsers, M. M. (2010) Fatty acid- and cholesterol transporter protein expression along the human intestinal tract. *PLoS ONE* **5,** e10380
22. Glatz, J. F., and van der Vusse, G. J. (1996) Cellular fatty acid-binding proteins: their function and physiological significance. *Prog. Lipid Res.* **35,** 243–282
23. Kimura, R., Takahashi, N., Goto, T., Murota, K., and Kawada, T. (2013) Activation of peroxisome proliferator-activated receptor-α (PPARα) in proximal intestine improves postprandial lipidemia in obese diabetic KK-Ay mice. *Obes. Res. Clin. Pract.* **7,** e353–e360
24. Kimura, R., Takahashi, N., Murota, K., Yamada, Y., Niiya, S., Kanzaki, N., Murakami, Y., Moriyama, T., Goto, T., and Kawada, T. (2011) Activation of peroxisome proliferator-activated receptor-α (PPARα) suppresses postprandial lipidemia through fatty acid oxidation in enterocytes. *Biochem. Biophys. Res. Commun.* **410,** 1–6
25. Srivastava, J., Robertson, C. L., Rajasekaran, D., Gredler, R., Siddiq, A., Emdad, L., Mukhopadhyay, N. D., Ghosh, S., Hylemon, P. B., Gil, G., Shah, K., Bhere, D., Subler, M. A., Windle, J. J., Fisher, P. B., and Sarkar, D. (2014) AEG-1 regulates retinoid X receptor and inhibits retinoid signaling. *Cancer Res.* **74,** 4364–4377
26. Mangelsdorf, D. J., Ong, E. S., Dyck, J. A., and Evans, R. M. (1990) Nuclear receptor that identifies a novel retinoic acid response pathway. *Nature* **345,** 224–229
27. Lefebvre, P., Benomar, Y., and Staels, B. (2010) Retinoid X receptors: common heterodimerization partners with distinct functions. *Trends Endocrinol. Metab.* **21,** 676–683
28. Heery, D. M., Kalkhoven, E., Hoare, S., and Parker, M. G. (1997) A signature motif in transcriptional co-activators mediates binding to nuclear receptors. *Nature* **387,** 733–736
29. Robertson, C. L., Srivastava, J., Siddiq, A., Gredler, R., Emdad, L., Rajasekaran, D., Akiel, M., Shen, X. N., Guo, C., Giashuddin, S., Wang, X. Y., Ghosh, S., Subler, M. A., Windle, J. J., Fisher, P. B., and Sarkar, D. (2014) Genetic deletion of AEG-1 prevents hepatocarcinogenesis. *Cancer Res.* **74,** 6184–6193
30. Bederman, I. R., Foy, S., Chandramouli, V., Alexander, J. C., and Previs, S. F. (2009) Triglyceride synthesis in epididymal adipose tissue: contribution of glucose and non-glucose carbon sources. *J. Biol. Chem.* **284,** 6101–6108
31. Lee, W. N., Bassilian, S., Guo, Z., Schoeller, D., Edmond, J., Bergner, E. A., and Byerley, L. O. (1994) Measurement of fractional lipid synthesis using deuterated water ($2H_2O$) and mass isotopomer analysis. *Am. J. Physiol.* **266,** E372–E383
32. Diraison, F., Pachiaudi, C., and Beylot, M. (1997) Measuring lipogenesis and cholesterol synthesis in humans with deuterated water: use of simple gas chromatographic/mass spectrometric techniques. *J. Mass Spectrom.* **32,** 81–86
33. Turley, S. D., Herndon, M. W., and Dietschy, J. M. (1994) Reevaluation and application of the dual-isotope plasma ratio method for the measurement of intestinal cholesterol absorption in the hamster. *J. Lipid Res.* **35,** 328–339
34. Clark, S. B., Ekkers, T. E., Singh, A., Balint, J. A., Holt, P. R., and Rodgers,

J. B., Jr. (1973) Fat absorption in essential fatty acid deficiency: a model experimental approach to studies of the mechanism of fat malabsorption of unknown etiology. *J. Lipid Res.* **14,** 581–588
35. Huynh, F. K., Green, M. F., Koves, T. R., and Hirschey, M. D. (2014) Measurement of fatty acid oxidation rates in animal tissues and cell lines. *Methods Enzymol.* **542,** 391–405
36. Ferré, P. (2004) The biology of peroxisome proliferator-activated receptors: relationship with lipid metabolism and insulin sensitivity. *Diabetes* **53,** S43–S50
37. Houten, S. M., and Wanders, R. J. (2010) A general introduction to the biochemistry of mitochondrial fatty acid β-oxidation. *J. Inherit. Metab. Dis.* **33,** 469–477
38. Chinetti, G., Lestavel, S., Bocher, V., Remaley, A. T., Neve, B., Torra, I. P., Teissier, E., Minnich, A., Jaye, M., Duverger, N., Brewer, H. B., Fruchart, J. C., Clavey, V., and Staels, B. (2001) PPAR-α and PPAR-γ activators induce cholesterol removal from human macrophage foam cells through stimulation of the ABCA1 pathway. *Nat. Med.* **7,** 53–58
39. Meng, X., Yang, S., Zhang, Y., Wang, X., Goodfellow, R. X., Jia, Y., Thiel, K. W., Reyes, H. D., Yang, B., and Leslie, K. K. (2015) Genetic deficiency of Mtdh in mice causes male infertility via impaired spermatogenesis and alterations in the expression of small non-coding RNAs. *J. Biol. Chem.* **290,** 11853–11864
40. Sohal, R. S., and Weindruch, R. (1996) Oxidative stress, caloric restriction, and aging. *Science* **273,** 59–63